Sensors and Materials, Vol. 31, No. 7 (2019) 2195–2212
MYU Tokyo

S & M 1924

Enhanced Sensitive Surface Acoustic Wave Device Designed for Nitric Oxide Gas Detection

Mei-Hui Chung,[1] Rey-Chue Hwang,[2] Jing-Jie Chiu,[2]
Min-Wen Yang,[2] Tien-Tsan Hung,[3] and Chi-Yen Shen[2*]

[1]Office of Institutional Research, I-Shou University,
No. 1, Sec. 1, Syuecheng Rd., Dashu District, Kaohsiung City 84001, Taiwan, R.O.C.
[2]Department of Electrical Engineering, I-Shou University,
No. 1, Sec. 1, Syuecheng Rd., Dashu District, Kaohsiung City 84001, Taiwan, R.O.C.
[3]Institute of Biotechnology and Chemical Engineering, I-Shou University,
No. 1, Sec. 1, Syuecheng Rd., Dashu District, Kaohsiung City 84001, Taiwan, R.O.C.

(Received November 13, 2018; accepted March 25, 2019)

Keywords: surface acoustic wave, gas sensor, nitric oxide, single-phase unidirectional transducer

Surface acoustic wave (SAW) devices equipped with an electrode-width-controlled (EWC)/single-phase unidirectional transducer (SPUDT) and fabricated on ST-X quartz were proposed and found to have low insertion loss and single-mode capability. The devices were then used to determine parts-per-billion levels of nitric oxide (NO). A new modified equivalent circuit (EC) model was used to model and analyze the characteristics of SAW devices prior to their fabrication. The small-signal frequency responses (S_{21}) obtained by simulation and measurement were consistent. A feedback-loop oscillator was used to design SAW-resonator-stabilized oscillators that provided stable oscillation. A SAW oscillator with an EWC/SPUDT structure was used to provide fundamental signals with high output power, induce high harmonic suppression, and realize long-term frequency stability. SAW devices with an EWC/SPUDT structure were coated with a Cu^{2+}/PANI/WO_3-sensitive layer to successfully determine parts-per-billion levels of NO. For a NO concentration of 50 ppb in dry air, the frequency shift in the SAW sensor with the EWC/SPUDT structure is 502 Hz. Moreover, the response and recovery time are 40 and 112 s, respectively. The sensitivity of NO detection for a concentration range of 20–80 ppb is approximately 4.2 Hz/ppb (~3.43 kHz/mg/m^3).

1. Introduction

Modern chemical sensors are designed to be highly sensitive and to efficiently transform chemical responses into measurable electronic signals. These devices should be designed such that they can be used for wireless communication and should be small to realize portable and miniaturized detection chips. Moreover, the accuracy of such sensors should be comparable to that of conventional analytical instruments. In environmental monitoring, personal safety, and industrial manufacturing, the detection of toxic or noxious gases at concentrations in parts-per-billion is crucial. Hydrogen sulfide (H_2S), for example, is a hazardous air pollutant and is

*Corresponding author: e-mail: cyshen@isu.edu.tw
https://doi.org/10.18494/SAM.2019.2195

ISSN 0914-4935

widely emitted during industrial processes such as oil and natural gas drilling and refining, sewage treatment, and paper milling.[1,2] H_2S can cause hypoxia and is hazardous for human health even when present in low concentrations. In February 2010, the American Conference of Governmental Industrial Hygienists adopted a new threshold limit recommendation for H_2S. They lowered the 8-h-time-weighted average for H_2S to 1.0 ppm. Moreover, the acceptable ambient limit for H_2S that is recommended by the Scientific Advisory Board on Toxic Air Pollutants of the United States is in the range of 20–100 ppb.[3] NO_x (NO and NO_2) in the environment is generated during the high-temperature combustion of fossil fuels. NO_x is a known component of photochemical smog and increases the risk of respiratory diseases in human beings.[4–6] Therefore, the NO concentration in ambient air should be monitored to examine and predict air quality, and provide public warning alerts. In physiopathology, the NO concentration in exhaled breath is used as a biomarker for monitoring inflammation in asthma patients.[7] The NO concentration ranges from 10 to 33 ppb in the exhaled breath of healthy adults. For patients with asthma, the NO geometric mean ranges from 6 to 98 ppb.[8,9] Therefore, it is crucial to fabricate sensing devices that can detect parts-per-billion levels of the gas with high sensitivity.

Various types of transducers, such as acoustic, thermal, and optical transducers, have been studied for the development of chemical sensors. Among the various types of sensing technologies, acoustic sensors have been particularly used for developing smart sensing devices because of their excellent actuation features.[10] Surface acoustic wave (SAW) devices are some of the most prominent acoustic devices used in chemical sensing applications. Since the interdigital transducer (IDT) was developed in 1965,[11] SAW technology has been widely used and studied for advancement. Owing to improvement in their design and fabrication, SAW devices are used in a wide range of radio frequency applications for frequency control, frequency selection, and signal processing. Currently, these devices are widely used in applications ranging from professional radar and communication systems to consumer applications such as mobile phones.

Because most SAW energy is trapped within a depth of 1.5 wavelengths on the surface of a material, SAWs are sensitive to variations in surface characteristics,[12] such as those in the mass loading effect, elastic properties, and acoustoelectric effect. In 1979, Wohltjen and Dessy developed gas sensors based on SAW oscillators that were structured using delay lines.[13] Since then, SAW devices have been found to be highly valuable for developing smart miniaturized sensors owing to their high sensitivity, small size, and rapid response. These devices have been applied in many studies for gas sensing.[14–21] Quartz is commonly used as a substrate for sensor applications because of its high temperature stability (temperature coefficient of delay, TCD~0) at room temperature (RT). However, the proposed SAW gas sensors using quartz substrates have high insertion loss because of bidirectional IDTs and the relatively weak piezoelectric coupling of quartz substrates. For effective detection, a practical SAW sensor should have a sufficiently large sensitive film area between the input and output IDTs. The long wave propagation distance between the input and output IDTs may result in a multimode response. Unfortunately, high insertion loss and multimode response are the primary factors that affect the frequency stability of the oscillator circuit with a SAW sensor.[22] Therefore, it is

difficult for a SAW sensor using a quartz substrate to achieve target detection in one step and when parts-per-billion levels of gas are present.

Sensitivity could be markedly enhanced using SAW sensors with higher operating frequencies. Therefore, SAW sensors with operating frequencies above 200 MHz were commonly employed.[6–10] Some studies have shown that SXFA-coated and BSP3-coated single-phase unidirectional transducer (SPUDT) SAW sensors with an operating frequency of 300 MHz detected DMMP in N_2 with sensitivities of 0.48 kHz/mg/m^3 (~2.42 kHz/ppm) in the concentration range of 2–14 mg/m^3 and 3.09 kHz/mg/m^3 (~15.45 kHz/ppm) in the concentration range of 1.5–8 mg/m^3, respectively.[15,16] These SPUDT SAW sensors had a threshold detection limit of less than 0.004 mg/m^3. In a previous study,[23] we developed a bidirectional λ/4-electrode transducer SAW sensor coated with a 0.2% Cu^{2+}/PANI/WO_3 sensitive layer that sensitively detected NO at ppb levels in dry air. In this work, a SPUDT SAW device working at frequencies below 100 MHz as well as having low insertion loss (less than 10 dB) and single-mode capability is proposed for detecting NO at a parts-per-billion level. A new modified equivalent circuit (EC) model, which is effectively developed by combining the EC model with the coupling-of-mode (COM) parameter model, was used to model and analyze the characteristics of the proposed SAW device. The performance of the proposed device was demonstrated by experiment. Subsequently, an oscillator circuit containing the SAW device in the feedback loop was configured for gas sensing. The change in oscillator frequency was monitored to investigate the detection properties of the sensor. The improved sensitivity, reversibility, and response time of a SAW sensor for detecting the parts-per-billion levels of NO were investigated in this study.

2. Design Considerations

2.1 SAW device

Various SPUDT configurations can be used to realize a SAW filter with low insertion loss due to the inherent unidirectivity of the SAW. The first SPUDT was proposed by Hanma and Hunsinger in 1976.[24] Since 1982, various SPUDT configurations, such as the double-metallization and floating-electrode SPUDT configurations, have been presented.[25–28] Studies have revealed that these SPUDT configurations not only reduce the insertion loss but also suppress triple-transit interference, flatten the passband ripple, and minimize the group delay ripple in SAW filters.

In this study, the electrode-width-controlled (EWC) SPUDT configuration was used in input and output IDTs to form a two-port resonator or a delay line for reducing the insertion loss and for multimode selection. The simulation result of frequency response is presented in Fig. 1 and reveals that the EWC/SPUDT structure enhances the signal power generated in the forward direction but reduces that in the reverse direction owing to the distributed reflection sources. The structure can suppress triple-transit interference that causes reflections within the transducers and can effectively reduce insertion loss.[24] On the other hand, transducers with a bidirectional λ/4-electrode width exhibit an antisymmetric radiation conductance response with

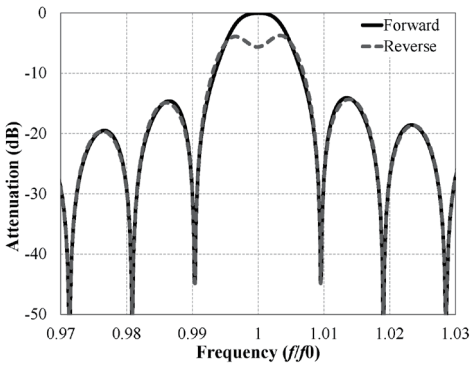

Fig. 1. Normalized forward and reverse frequency responses of pure EWC/SPUDT transducers (length is 105λ).

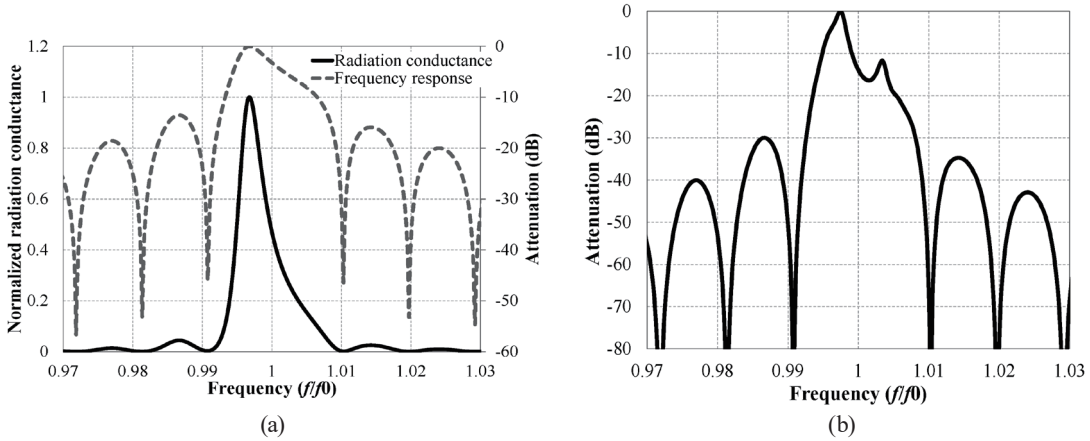

Fig. 2. (a) Normalized radiation conductance and frequency responses of bidirectional λ/4-electrode transducers (length is 105λ) and (b) the frequency response of the device with the length of input and output bidirectional λ/4-electrode transducers of 105λ.

respect to the center frequency, as displayed in Fig. 2(a), and may affect the frequency response of the device, as illustrated in Fig. 2(b). Conversely, the normalized radiation conductance response of the transducers with the EWC-SPUDT structure is symmetric with respect to the center frequency. Thus, the EWC/SPUDT transducer exhibits a higher frequency performance, as indicated in Fig. 3, than the bidirectional λ/4-electrode transducer.

A long distance was designed between the input and output transducers so that a sensitive film could be deposited to enable effective detection. However, a long distance may deteriorate device performance and multimode response. Owing to the multimode response, the oscillator may induce frequency mode hopping, and the stability of the oscillator is also affected. To predict device performance, a new modified EC method was proposed in this study to model and analyze the characteristics of SAW devices prior to their fabrication. The COM theory and EC are widely used in analyzing SAW devices. Both methods show some advantages and disadvantages. For example, the model using the COM theory requires less time for executing a program but requires some effort to derive equations and parameters for different IDT structures.[29] By contrast, the EC is very flexible and thus easily fits various IDT structures; nevertheless, the calculation requires a higher number of iterations to form electrodes in an organized manner,

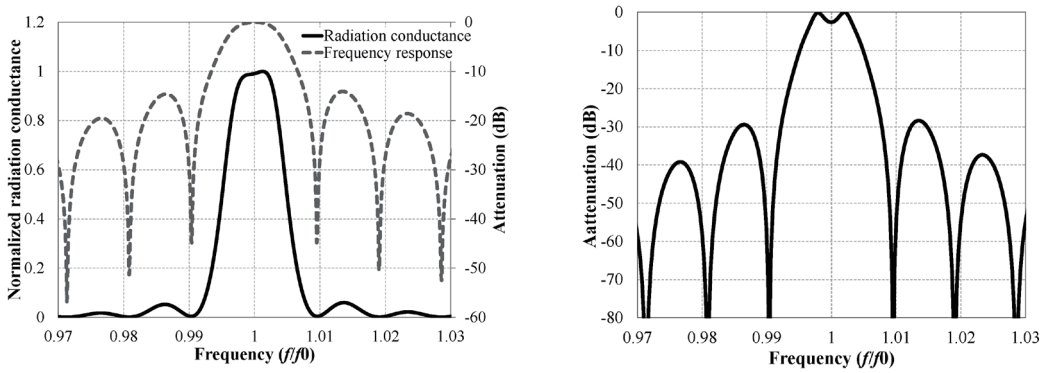

(a) (b)

Fig. 3. (a) Normalized radiation conductance and frequency response of EWC/SPUDT transducers (length is 105λ) and (b) the frequency response of the device with the length of input and output EWC/SPUDT transducers of 105λ.

thus requiring a long execution time.[30] In this study, the COM and EC models were combined to employ their different advantages by developing a new modified EC model that converted COM parameters into EC parameters with a metallization ratio of 0.5. Then, the EC parameters were used for modeling various IDT structures with metallization ratios other than 0.5. This new modified EC method was applied to the design of SAW sensors with EWC/SPUDT structures in this study.

As shown in Fig. 4, the parameters Z_0, Z_m, jB, and C_S should be determined in advance to simulate the SAW using Mason's EC model. Here, L_s and L_g are the lengths of the metallized and unnmetallized portions, Z_m and Z_0 are the characteristic impedances of these portions, and γ_m and γ_0 are the propagation constants under these portions, respectively. By using the finite-element method and spectral domain analysis (FEMSDA),[31] the software developed by Hashimoto, the following COM parameters were calculated and extracted at a metallization ratio of 0.5: the velocity of the slow-shear surface skimming bulk wave (SSBW), V_B, the dielectric constant $\varepsilon(\infty)$, the propagation loss α, the electromechanical coupling factor k^2, the parameter determining the reflection of the SAWs, ε, the penetration depth of the SAWs, η, and $c = V_B/V_{ref}$ (where V_{ref} is the SAW velocity for reference). Then, by considering the approximate dispersion relation proposed by Plessky[32] and the dispersion relation of short-circuited grating, the detune factor θ_u and reflection coefficient per period for the short-circuited coefficient, κ_{12}, were calculated using the COM parameters.[33] The detune factor is expressed as

$$\theta_u = \frac{\omega}{V_{ref}} - \frac{M\pi}{p} + \kappa_{11}, \tag{1}$$

where κ_{11} is the self-coupling coefficient corresponding to the phase shift per period of the short-circuited grating without reflection, p is the length of a unit cell of each electrode, and M is the Bragg reflection of the Mth order. The characteristic impedance of the metallized portion in the EC model that is obtained by conversion from the COM parameters is $Z_m = 1 - \kappa_{12}p$ when

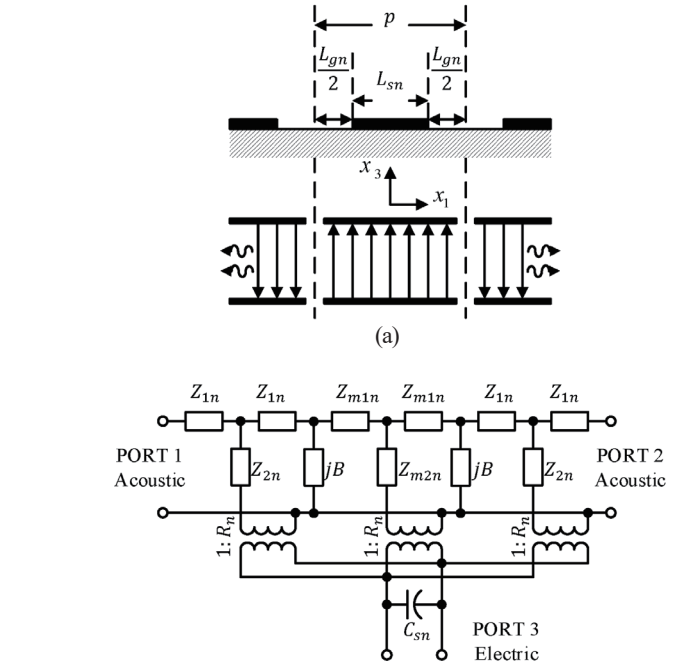

Fig. 4. (a) Cross-field model for a single electrode of the IDT and (b) three-port Mason's EC of a single electrode including an acoustic impedance discontinuity.

$Z_0 = 1$. The susceptance element jB connected in parallel at the electrode edges is responsible for the energy storing effect. In the energy storing effect, the energy of a scattered BAW is stored near the strip edge. The effect causes a reduction in SAW velocity. The relationship between the susceptance element and the self-coupling coefficient is as follows: $jB = j\kappa_{11}p$. Cs is the static capacitance of a single electrode and is given by

$$C_s = \frac{W\varepsilon(\infty)\varepsilon_0}{2}\frac{K(q)}{K(q')}, \tag{2}$$

where W is the width of the acoustic aperture of the electrode, ε_0 is the dielectric constant of air, and K is the Jacobian complete elliptic integral of the first kind with $q = \sin(\pi L_s/2p)$ and $q' = \sqrt{(1-q^2)}$. The transformer ratio R_n is obtained using

$$R_n = (-1)^n \sqrt{2 f_a C_s k^2 Z_0}\left[\frac{K(2^{-\frac{1}{2}})}{K(q)}\right]. \tag{3}$$

The average shifted center frequency f_a [30] of the periodic transducer configuration is given as $f_a = v_a/2p$. Moreover, the average shifted velocity v_a under an IDT due to metallization can be expressed as $v_a = v_{ref}(1 - \kappa_{11}p/\pi)$.

Figures 5(a) and 5(b) illustrate the results obtained when the COM approach and new modified EC model were used to calculate the reflection coefficient of a reflection grating, and the transduction response between the electric and acoustic ports of an IDT at a metallization ratio of 0.5, respectively. As indicated in the figures, the results obtained using the two methods are in agreement. The element factor presented in Fig. 6 is the ratio of the excitation efficiency for each period of the IDT relative to the best one.[33] The element factors obtained using the new modified EC model are consistent with those in another study.[33] This proves that the new modified EC model is suitable for modeling and analyzing the characteristics of SAW devices.

2.2 Feedback-loop oscillator design

When specific gas molecules are absorbed on the sensitive layer coated on the wave propagation path of an SAW sensor, SAW propagation is perturbed. A change in SAW propagation can be evaluated by measuring the frequency shift in the SAWs. Hence, the

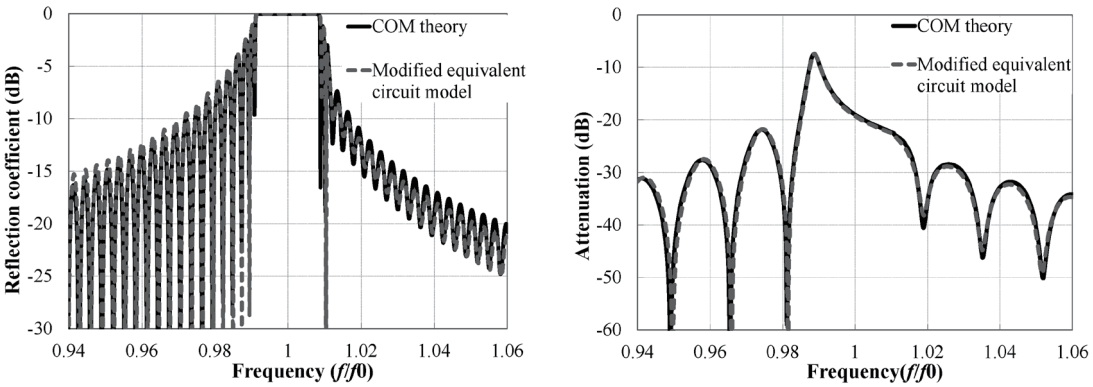

(a) (b)

Fig. 5. (a) Reflection coefficient of a reflection grating and (b) transduction response between electric and acoustic ports of an IDT at metallization ratio of 0.5.

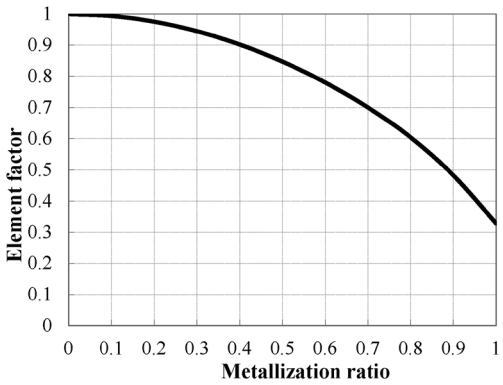

Fig. 6. Element factor versus metallization ratio calculated by using the modified RT model.

oscillator circuit with the SAW device in the feedback loop was selected for this study; its architecture is presented in Fig. 7. The oscillator consists of a loop amplifier, a two-port SAW device, and a loop gain or phase adjust circuit, and a signal sampling circuit fabricated using lumped components. The oscillation presents a closed loop gain initially, and the oscillation phase satisfies Barkhausen's criteria:

$$\Sigma\,(G_{amp}, G_{saw}, D_{adj}) \geq 1 \tag{4}$$

and

$$\theta_{amp} + \theta_{saw} + \theta_{adj} = 2\pi N, \tag{5}$$

where G_{amp} and θ_{amp} are the gain and phase change of the loop amplifier, and G_{saw} and θ_{saw} are the loss and phase change of the two-port SAW device, respectively; G_{adj} is the total loss of the loop gain or phase adjust circuit and signal sampling circuit; and θ_{adj} is the total phase change in the circuits.

3. Experimental Methods

3.1 Materials and reagents

Aniline monomer was obtained from ACROS (Bergen County, NJ, USA) and distilled prior to use. Tungsten hexachloride (WCl_6, Aldrich, St Paul, MN, USA), ammonium persulfate [$(NH_4)_2S_2O_8$, Showa, Tokyo, Japan], hydrogen chloride (HCl, Union Chemical Works Ltd., Hsinchu, Taiwan), isopropanol (TEDIA, Fairfield, OH, USA), copper sulfate ($CuSO_4$, Aldrich), and ammonium hydroxide (NH_4OH, TEDIA) were used without pretreatment. All chemicals used were of the analytical reagent grade. NO gases with concentrations of 116 and 300 ppb were obtained from Jing-De Gas Co. (Kaohsiung, Taiwan).

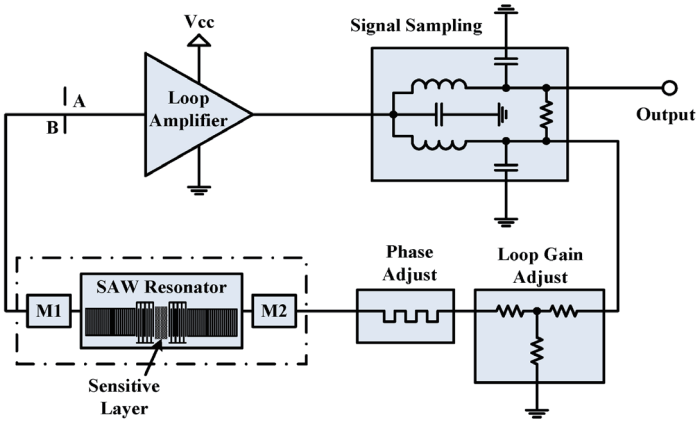

Fig. 7. Block diagram of a feedback-loop oscillator.

3.2 Preparation of Cu^{2+}/PANI/WO_3 films

The procedure employed to prepare Cu^{2+}/PANI/WO_3 solution was similar to that employed in our previous studies.[23] Tungsten oxide gel was first synthesized and then mixed with an aniline precursor. Tungsten (VI) hexachloride was mixed with isopropanol in an ice bath, and then, hydrolysis occurred at RT. The solution was subsequently gelled using NH_4OH. Aniline monomer (0.1 mol) was dissolved in 1 M HCl and mixed with tungsten oxide gel by stirring vigorously. The aniline solution was polymerized by adding ammonium persulfate; the solution was then maintained at RT for 20 h. Subsequently, the obtained PANI/WO_3 precipitate was rinsed in deionized water and then washed with 1 M HCl solution. The derived solution was mixed with isopropanol, which facilitated the deposition of the sensitive layer. Moreover, the obtained PANI/WO_3 solution was mixed with appropriate amounts of $CuSO_4$ aqueous solution to prepare copper-ion-doped PANI/WO_3 films with 0.3 wt% Cu^{2+}.

3.3 SAW sensor measurement

The sensing properties of the fabricated SAW sensors were evaluated within an enclosure containing NO at various concentrations. Figure 8 shows the setup applied in the NO measurement experiment. Mass flow controllers (Sierra, Kyoto, Japan) were used to prepare the required set of gas dilutions by using certified NO of 116 ppb and dry air cylinders (Jing-De Gas Co., Kaohsiung, Taiwan). NO and dry air were transported using mass flow controllers equipped with a precision mass flow meter (Sierra) to change the ratio of NO gas to dry air. A NO sensor (FENO, Bedfont, UK) was used to independently confirm the NO concentration in the gases generated using this dilution method. The outflow was controlled at a constant flow rate of 110 mL/min during the measurements. Dual-track sensors were placed in a sealed 5 cm^3 test chamber with a stable temperature. A temperature controller was used to maintain a constant temperature of 23 °C.

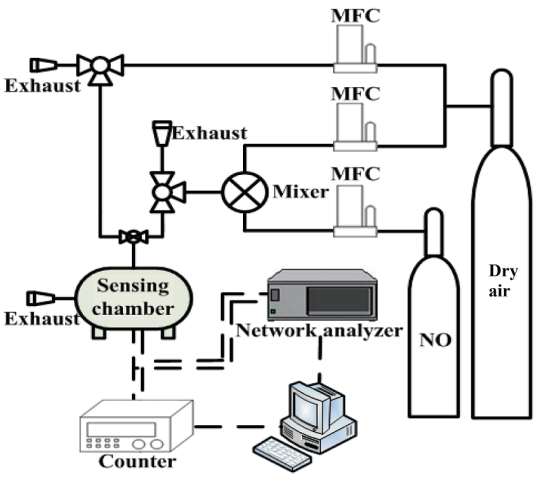

Fig. 8. (Color online) Experimental setup for NO measurement.[34]

The frequency of the SAW sensors was continually monitored using a frequency counter (53132A, Agilent, USA) connected to a computer through a GPIB interface. Before the transient frequency response of a sensor to NO was measured, the gas sensor was exposed to a dry air stream for 30 min to eliminate unwanted gas molecules and stabilize the background signal. Each NO pulse comprised 180 s NO exposure followed by 30 min dry air purge. The sensor response was defined as the variation in the operating frequency of the SAW sensor due to NO adsorption. The frequency shifts in all experiments were calculated on the basis of the average response of the reactions, and the corresponding standard deviations of triplicate measurements were calculated.

4. Results and Discussion

4.1 SAW device

In this study, the SAW sensor was designed as a two-port resonator or a delay line with an operating frequency of approximately 98.3 MHz (period: 32 μm) and fabricated on an ST-X quartz substrate. The geometric parameters of the fabricated SAW devices are listed in Table 1. The aperture was 1 mm (31λ), the distance between the input and output transducers was approximately 600 μm, and aluminum IDTs with a thickness of 3200 Å were produced using the lift-off method. To reduce interference from the environment, a dual-device configuration was used, as illustrated in Fig. 9, and the size of the device was approximately 15.3 × 5.8 mm^2.

As shown in Figs. 10 and 11, the simulation and measurement (obtained using an Agilent 85033E network analyzer) results for devices D1 and D2 are consistent. The frequency responses of devices D1 and D2 reveal low insertion losses of 8.6 and 9.2 dB, respectively, and linear phase changes at the 3 dB frequency bandwidth. The insertion losses of devices D1 and

Table 1
Geometric parameters of SAW devices.

Device	D0	D1	D2
Device structure	Two-port resonator	Two-port resonator	Delay line
Length of input transducers	106λ	106λ	185λ
Length of output transducers	106λ	106λ	185λ
Configuration of transducers	bidirectional λ/4-electrode	EWC/SPUDT	EWC/SPUDT
Number of strip gratings	150	150	—

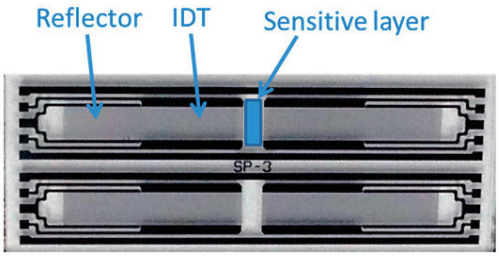

Fig. 9. (Color online) Photograph of a dual-device configuration.

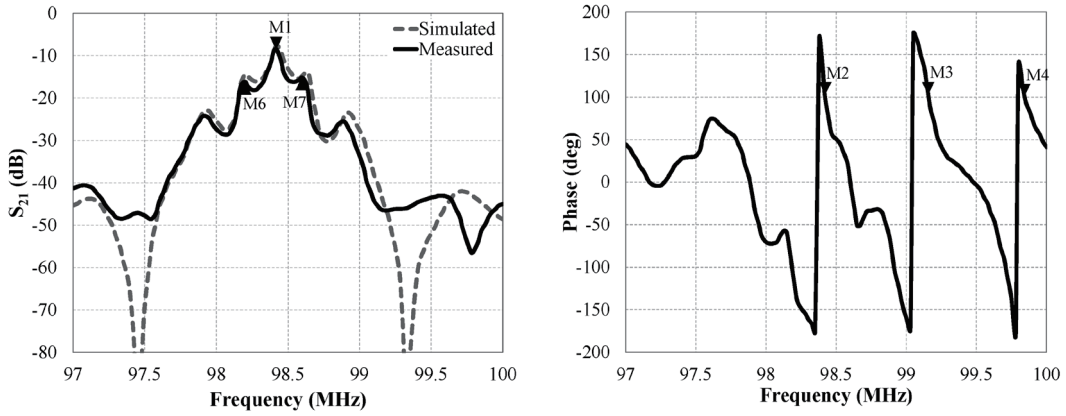

(a) (b)

Fig. 10. Frequency response of SAW two-port resonator with EWC/SPUDT transducers (device D1) under matched conditions: (a) simulated and measured amplitude responses and (b) measured phase response.

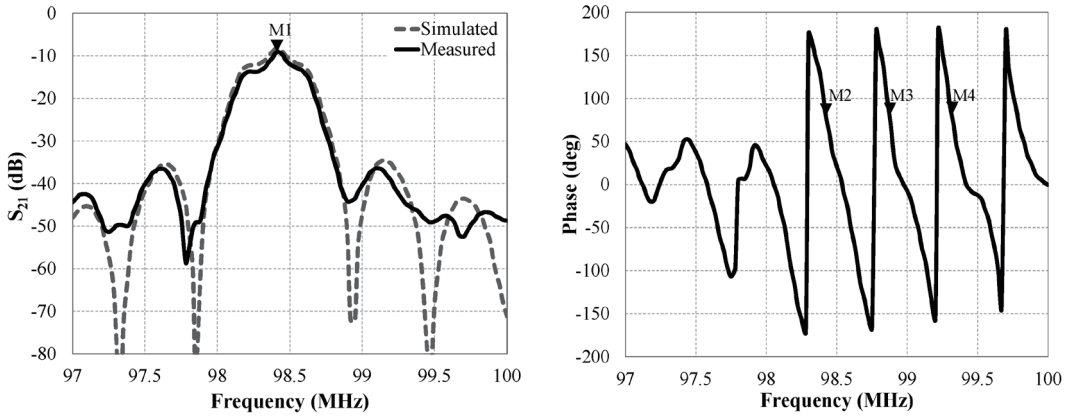

(a) (b)

Fig. 11. Frequency response of SAW delay line with EWC/SPUDT transducers (device D2) under matched conditions: (a) simulated and measured amplitude responses and (b) measured phase response.

D2 were slightly lower than that of device D0. The frequency and phase responses reveal that the oscillation criteria are only satisfied at the center frequency; that is, there are minimum losses at this frequency [M1 in Figs. 10(a) and 11(a)]. The corresponding phase is marked as M2 in Figs. 10(b) and 11(b). Although there is a phase shift of 2π and the oscillator criterion is met [M3 or M4 in Figs. 10(b) and 11(b)], the corresponding insertion loss is 10 dB higher than the loss in the primary mode. Similarly, if the insertion losses of other modes in the passband meet the oscillator criterion [M6 or M7 in Fig. 10(a)], the modes do not satisfy the oscillation phase criterion. This finding indicates that the EWC/SPUDT structure enhances the single-mode selection, and thus, the oscillator works at a single frequency.

4.2 SAW oscillator

The oscillator circuit with the SAW sensor in the feedback loop was selected for this study, and its architecture is presented in Fig. 7. The output and input ports of the SAW sensor were connected by an oscillator circuit, which was fabricated using discrete elements integrated into a circuit board. The discrete elements included a two-stage amplifier with a gain of more than 30 dB, a 3 dB lump-element reactive Wilkinson power splitter, and a lumped-element phase adjuster. The performance of the oscillator was measured using a spectrum analyzer (N9010A, Agilent). The narrow and wide scans of the output spectrum of oscillators D1 are presented in Fig. 12, and the output parameters of three oscillators are listed in Table 2. Compared with oscillator D0, oscillators D1 and D2 (which include EWC/SPUDTs) have a fundamental signal with higher output power and exhibit superior harmonic level suppression. This implies that the EWC/SPUDT configuration effectively guides the SAW energy transmission between the input and output IDTs and suppresses the level of the harmonics.

Frequency stability is considered a key factor affecting the sensitivity of a sensor. Temperature change or oscillator aging generally results in changes in oscillator frequency over time. For good oscillators, this instability is measured in parts per million. The long-term stabilities of the oscillators are summarized in Table 2. The long-term frequency drifts in these oscillators were measured over 24 h. The devices that employ the EWC-SPUDTs exhibit a higher oscillator performance, which is characterized by output power, harmonic level suppression, and long-term frequency stability, than the devices that employ the $\lambda/4$-electrode transducers.

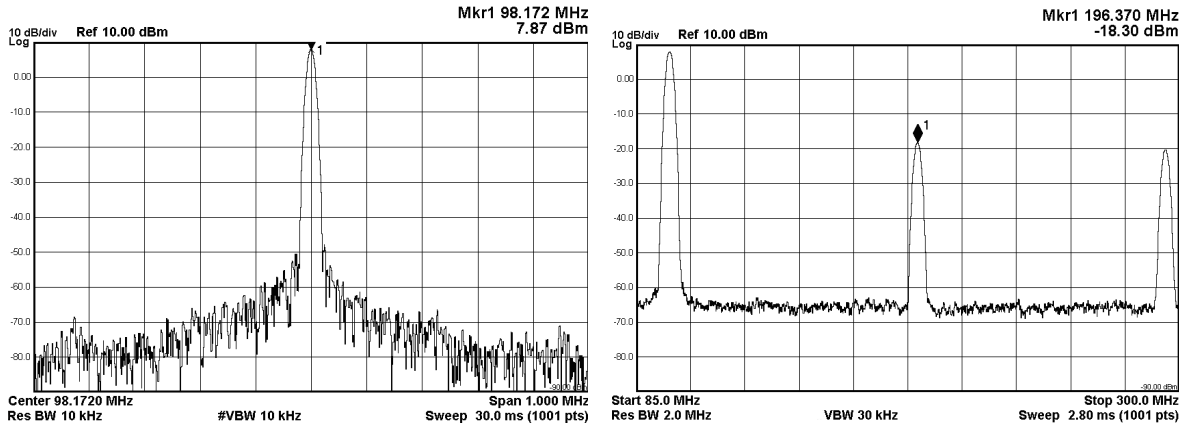

(a) (b)

Fig. 12. (a) Measured output spectrum for operating frequency of 98.3 MHz and (b) harmonics spectrum of SAW two-port resonator with EWC/SPUDT transducers (device D1).

Table 2
Output parameters and frequency stabilities of oscillators.

Device	D0	D1	D2
Output power of fundamental (dBm)	6.95	7.87	7.42
Relative level of 2nd harmonic (dBm)	−18.51	−26.17	−19.24
Long-term stability (ppm)	1.17	0.36	0.66

4.3 SAW sensor

As aforementioned, NO detection is crucial in medical applications. The aim of this study was to develop a SAW sensor for detecting parts-per-billion levels of NO at RT. To this end, a dual-track configuration was used to reduce environmental interference. A sensing track was obtained by spin-coating a 1.5 × 0.5 mm^2 sensitive 0.3%-Cu^{2+}/PANI/WO_3 layer between two IDTs; no sensitive layer was deposited on the reference track surface. The thickness of the Cu^{2+}/PANI/WO_3 sensitive layer was measured to be approximately 3000 Å by ellipsometry. It was reported in Ref. 23 that the Cu^{2+}/PANI/WO_3 sensitive layer had a porous structure and could detect NO.

Figure 13 displays the responses of the developed SAW sensors when exposed to 50 ppb NO in dry air at RT. The frequency response of the SAW sensors increases during NO exposure and is reversible. The perturbation mechanisms of SAW propagation after the adsorption of gas targets can be expressed as[35]

$$\frac{\Delta f}{f_0} \cong \frac{\Delta v}{v_0} = -c_m f_0 \Delta\left(\frac{m}{A}\right) + 4c_e f_0 (\Delta h G') - \frac{k^2}{2}\Delta\left(\frac{\sigma_s^2}{\sigma_s^2 + v_0^2 C_s^2}\right), \tag{6}$$

where c_m and c_e are the coefficients of mass sensitivity and elasticity, respectively, m/A is the change in mass per unit area, h is the thickness of the sensitive layer, G' is the shear modulus, k^2 is the electromechanical coupling coefficient, and σ_s is the sheet conductivity of the sensitive layer. The first term on the right-hand side of Eq. (6) represents the mass loading effect that results in negative frequency shifts and is a function of NO concentration. The second term is the contribution of the elastic properties of the sensitive layer. The frequency shift resulting from the elastic effect is positive. The third term represents the acoustoelectric effect. The frequency shift due to the acoustoelectric response is positive because NO was a reducing gas at RT in this study.[35] The frequency shift during exposure to NO in dry air, as illustrated

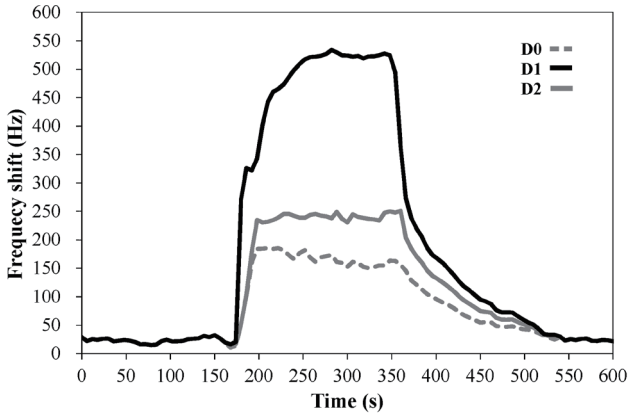

Fig. 13. Response of a SAW sensor coated with a 0.3% Cu^{2+}/PANI/WO_3 sensing film to 50 ppb NO in dry air at RT.

in Fig. 13, was positive, indicating that the elastic and acoustoelectric effects of the sensitive layers outweighed the mass loading effect. Therefore, the modification of the elastic and acoustoelectric effects led to increases in oscillation frequency.

Figure 13 also reveals that both EWC/SPUDT SAW sensors, which are devices D1 and D2, exhibit higher responses than the bidirectional $\lambda/4$-electrode transducer SAW sensor during NO adsorption. For a NO concentration of 50 ppb in dry air, the frequency shift in the EWC/SPUDT SAW resonator is 502 Hz. Moreover, the response time and recovery time, which are defined as the time required for the response signal to rise to 90% of its maximum after the beginning of gas exposure and the time required for the response signal to return to 90% of the original baseline signal upon removal of target gas, respectively, were calculated. The experimental results are listed in Table 3 and reveal that the response time is less than 1 m and that the recovery time is about 2 min at a NO concentration of 50 ppb in dry air.

Devices D0 and D1, which both have a two-port resonator structure, were next exposed to various NO concentrations to evaluate sensitivity. The sensor response increases with NO concentration, as plotted in Fig. 14. The sensitivity of device D1 was evaluated to be approximately 4.2 Hz/ppb (~3.43 kHz/mg/m^3), which is approximately three times higher than that of device D0 (~1.5 Hz/ppb) for NO concentrations in the range of 20–80 ppb. These results indicate that the developed EWC/SPUDT SAW sensor exhibited accurate parts-per-billion-level detection, optimal reversibility, and rapid response to NO at RT.

Table 4 shows some of the SAW NO_x sensors reported in the literature.[36–38] Compared with other SAW sensors in early works, the frequency response in the present work is significant towards 20 ppb NO concentration. Hence, the present EWC/SPUDT SAW sensor coated with a Cu^{2+}/PANI/WO_3 layer is able to sensitively detect NO gas concentrations of the order of parts-per-billion at room temperature.

Table 3
Experimental results of gas sensors to 50 ppb NO in dry air at RT.

Device	D0	D1	D2
Frequency shift (Hz)	128	502	211
Response time (s)	12	40	15
Recovery time (s)	139	112	138

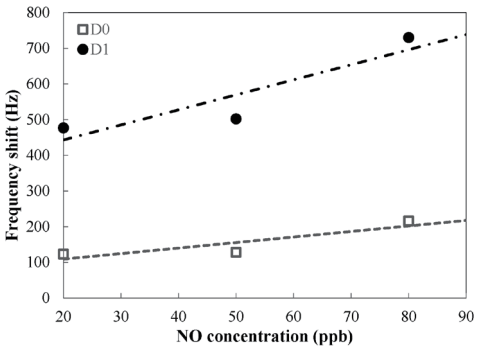

Fig. 14. Frequency shifts of the sensor in response to various NO concentrations in dry air at RT.

Table 4
Comparison of different SAW sensors reported in the literature.

Sensing film	Target gas	Operating temperature	Operating frequency	Gas concentration	Sensor response	Reference
SnO_2	NO_2	RT	433.92 MHz	20 ppm	~30 MHz	[36]
ZnO	NO_2	RT	99.5 MHz	400 ppb	6 kHz	[37]
PZT	NO_2	RT	99.4 MHz	80 ppm	1.11 kHz	[38]
Cu^{2+}/PANI/WO_3	NO	RT	98.3 MHz	20 ppb	477 Hz	This work

An EWC/SPUDT SAW resonator using a Cu^{2+}/PANI/WO_3 sensitive layer exhibited a detection sensitivity of 4.2 Hz/ppb for detecting NO in the concentration range of 20–80 ppb. In the future, the development and improvement of SAW sensors for detecting parts-per-billion levels of gases will be continued for subsequent medical applications.

5. Conclusions

In this study, the new modified EC model was used to model and analyze the characteristics of SAW devices prior to their fabrication. The simulation and measurement results were consistent. The EWC/SPUDT configuration enhanced single-mode selection, effectively guided the SAW energy transmission between the input and output IDTs, and suppressed the harmonic level. SAW oscillators fabricated on an ST-X quartz substrate with an EWC/SPUDT structure could be operated at a single frequency and provided a higher-output-power fundamental signal, superior harmonic level suppression, and long-term frequency stability compared with those without the structure. The experimental results obtained using the gas sensor revealed that a SAW sensor has superior sensitivity, responds rapidly, and requires a short recovery time for detecting parts-per-billion levels of NO in dry air at RT. An EWC/SPUDT SAW resonator using a Cu^{2+}/PANI/WO_3 sensitive layer exhibited a detection sensitivity of 4.2 Hz/ppb for detecting NO in the concentration range of 20–80 ppb. In the future, the development and improvement of SAW sensors for detecting parts-per-billion levels of gases will be continued for subsequent medical applications.

Acknowledgments

The authors thank the Ministry of Science and Technology, Taiwan, for partially supporting this research under Contract No. MOST106-2221-E-214-028.

References

1 J. Ma, Y. Liu, H, Zhang, P. Ai, N. Gong, Y. Wu, and D. Yu: Sens. Actuators, B **216** (2015) 72. https://doi.org/10.1016/j.snb.2015.04.025
2 Z. Li, Y. Huang, S. Zhang, W. Chen, Z. Kuang, D. Ao, W. Liu, and Y. Fu: J. Hazard. Mater. **300** (2015) 167. https://doi.org/10.1016/j.jhazmat.2015.07.003
3 Y. S. Patil, F. C. Raghuvanshi, and I. D. Patil: Int. J. Sci. Res. **7** (2016).
4 K. Izumi, M. Utiyama, and Y. Y. Maruo: Sens. Actuators, B **216** (2015) 128. https://doi.org/10.1016/j.snb.2015.04.029
5 A. T. Dinh-Xuan, I. Annesi-Maesano, P. Berger, A. Chambellan, P. Chanez, T. Chinet, B. Degano, C. Delclaux, V. Demange, A. Didier, G. Garcia, A. Magnan, B. Mahut, and N. Roche: Rev. Mal. Respir. **32** (2015) 193. https://doi.org/10.1016/j.rmr.2014.11.004
6 S. Bennett: Medium/Heavy Duty Truck Engines, Fuel & Computerized Management Systems (Cengage Learning, New York, 2016) p. 392.
7 H. K. Gattya, S. Leijonmarckb, M. Anteliusa, G. Stemmea, and N. Roxhed: Sens. Actuators, B **209** (2015) 639. https://doi.org/10.1016/j.snb.2014.11.147
8 N. M. Grob and R. A. Dweik: J. Breath Res. **2** (2008) 3. https://doi.org/10.1088/1752-7155/2/3/037002
9 R. A. Dweik, P. B. Boggs, S. C. Erzurum, C. G. Irvin, M. W. Leigh, J. O. Lundberg, A. Olin, A. L. Plummer, and D. R. Taylor: Am. J. Respir. Cri. Care Med. **184** (2011) 5. https://doi.org/10.1164/rccm.9120-11ST
10 M. Hussain, F. Rupp, H. P. Wendel, and F. K Gehring: Trends Analyt. Chem. **102** (2018) 194. https://doi.org/10.1016/j.trac.2018.02.009

11 R. M. White and F. M. Voltmer: Appl. Phys. Lett. **7** (1965) 314.
12 A. Mujahid and F. L. Dickert: Sensors **17** (2017) 2716. https://doi.org/10.3390/s17122716
13 H. Wohltjen and R. Dessy: Anal. Chem. **51** (1979) 1458.
14 A. Tretjakov, V. Syritski, J. Reut, R. Boroznjak, and A. Öpik: Anal. Chim. Acta **902** (2016) 182. https://doi.org/10.1016/j.aca.2015.11.004
15 D. Sil, J. Hines, U. Udeoyo, and E. Borguet: Appl. Mater. Interfaces **7** (2015) 5709. https://doi.org/10.1021/am507531s
16 W. Wang, H. Hu, G. Chen, X. Xie, and S. He: IEEE Sens. J. **15** (2015) 6730. https://doi.org/10.1109/JSEN.2015.2464790
17 S. Y. Wang, J. Y. Ma, Z. J. Li, H. Q. Su, N. R. Alkurd, W. L. Zhou, L. Wnag, B. Du, Y. L. Tang, D. Y. Ao, S. C. Zhang, Q. K. Yu, and X. T. Zu: J. Hazard. Mater. **285** (2015) 368. https://doi.org/10.1016/j.jhazmat.2014.12.014
18 Z. Yunusa, M. N. Hamidon, A. Ismail, M. M. Isa, M. H. Yaacob, S. Rahmanian, S. A. Ibrahim, and A. A. A. Shabaneh: Sensors **15** (2015) 4749. https://doi.org/10.3390/s150304749
19 W. Wang, H. Hu, X. Liu, S. He, Y. Pan, C. Zhang, and C. Dong: Sensors **16** (2016) 73. https://doi.org/10.3390/s16010073
20 J. Devkota, P. R. Ohodnicki, and D. W. Greve: Sensors **17** (2017) 801. https://doi.org/10.3390/s17040801
21 L. Rana, R. Gupta, M. Tomar, and V. Gupta: Sen. Actuators, B **252** (2017) 840. https://doi.org/10.1016/j.snb.2017.06.075
22 M. F. Lewis: Proc. 28th Annu. Freq. Control Symp. (IEEE, 1974) 304–314.
23 S. H. Wang, C. Y. Shen, Z. J. Lien, and J. H. Wang: Sens. Actuators, B **243** (2017) 1075. https://doi.org/10.1016/j.snb.2016.12.101
24 K. Hanma and B. J. Hunsinger: Proc. 1976 Ultrason. Symp. (IEEE, 1976) 328–331. https://doi.org/10.1109/ULTSYM.1976.196692
25 A. Winkler, R. Brünig, C. Faust, R. Weser, and H. Schmidt: Sen. Actuators, A **247** (2016) 259. https://doi.org/10.1016/j.sna.2016.06.006
26 F. Q. Xu, W. Wang, X. F. Xue, H. L. Hu, X. L. Liu, and Y. Pan: Sensors **15** (2015) 30187. https://doi.org/10.3390/s151229793
27 X. Sun, W. Liu, X. Shao, S. Zhou, W. Wang, and D. Lin: Sensors **19** (2019) 106. https://doi.org/10.3390/s19010106
28 X. Zhao, R. Shi, Y. Yang, P. Qin, Y. Ma, and Y. Wen: Proc. 2017 IEEE Int. Ultrason. Symp. (IEEE, 2017) https://doi.org/10.1109/ULTSYM.2017.8092729
29 G. Tang, T. Han, J. Chen, B. Zhang, T. Omori, and K. Hashimoto: Jpn. J. Appl. Phys. **55** (2016) 07KD09-1~5.
30 N. J. Mukhtar, N. A. Aziz, and B. Bais: Proc. 2016 IEEE Int. Conf. Semicond. Electr. (IEEE, 2016) https://doi.org/10.1109/SMELEC.2016.7573590
31 Y. Sakamoto, K. Hashimoto, and M. Yamaguchi: J. J. Appl. Phys. **37** (1998) 2905.
32 V. Plessky: Proc. 1993 IEEE Ultrason. Symp. (IEEE, 1993) 195–200. https://doi.org/10.1109/ULTSYM.1993.339679
33 R. C. M. Li and J. Melngailis: IEEE Trans. Sonics Ultrason. **22** (1975) 189. https://doi.org/10.1109/T-SU.1975.30797
34 S. H. Wang, C. Y. Shen, J. M. Su, and S. W Chang: Sensors **15** (2015) 7084. https://doi.org/10.3390/s150407084
35 S. H. Wang, C. Y. Shen, Z. J. Lien, and J. H. Wang: Sen. Actuators, B **243** (2017) 1075. https://doi.org/10.1016/j.snb.2016.12.101
36 V. B. Raj, A. T. Nimal, M. Tomar, M. U. Sharma, and V. Gupta: Sens. Actuators, B **220** (2015) 154. https://doi.org/10.1016/j.snb.2015.05.043
37 L. Rana, R. Gupta, M. Tomar, and V. Gupta: Sens. Actuators, B **252** (2017) 840. https://doi.org/10.1016/j.snb.2017.06.075
38 L. Rana, R. Gupta, R. Kshetrimayum, M. Tomar, and V. Gupta: Surf. Coat. Technol. **343** (2018) 89. https://doi.org/10.1016/j.surfcoat.2017.10.077

About the Authors

Mei-Hui Chung received her M.S. and Ph.D. degrees in Electrical Engineering from I-Shou University in Taiwan in 2000 and 2007, respectively. She currently serves as a section chief of Institutional Research at I-Shou University, Taiwan. Her research interests are in surface acoustic wave device design and high-frequency circuit design. (mhchung@isu.edu.tw)

Rey-Chue Hwang received his Ph.D. degree in Electrical Engineering from Southern Methodist University, Dallas, TX, in 1993. Currently, he is a full professor of Electrical Engineering Department, I-Shou University, Taiwan, R.O.C. Dr. Hwang has published more than 250 papers in various journals and conferences in the areas of artificial intelligent system, signal processing, and fuzzy control. He is now a Fellow of IET and a senior member of IEEE. He chartered the IEEE CIS Chapter, Tainan Section and served as the co-chair and chair from years 2004 to 2009. (rchwang@isu.edu.tw)

Jing-Jie Chiu received his B.S. degree in Electrical Engineering from I-Shou University in 2017 and is currently in the M.S. program of Electrical Engineering, I-Shou University. (c90041912@gmail.com)

Min-Wen Yang received his B.S. degree in Electrical Engineering from I-Shou University in 2017 and is currently in the M.S. program of Electrical Engineering, I-Shou University. (caramelcool0318@gmail.com)

Tien-Tsan Hung is an associate professor of the Institute of Biotechnology and Chemical Engineering at I-Shou University. His work focuses specifically on the design and synthesis of organic electro-optics materials and related devices. His related research works include the molecular design and preparation of modified organic electro-optics materials, structure characterization, physical property measurements, and electric property testing of related devices. On-going research topics are dye-sensitized solar cells, organic-inorganic hybrid materials, and nanocomposites. (tthung@isu.edu.tw)

Chi-Yen Shen received her B.S. degree in Electrical Engineering from Cheng-Kung University in Taiwan in 1987 and Ph.D. degree in Electrical Engineering from National Sun Yat-Sen University in Taiwan in 1991. In 1991, she was employed as an associate professor of Electrical Engineering at Kaoshiung Ploytechnic Institute, Taiwan. She is currently a professor of Electrical Engineering at I-Shou University, Taiwan. Her research interests are in surface acoustic wave devices, sensors, and electronic ceramics.